

Disk-Corona Model in Active Galactic Nuclei: an Observational Test*

Fang Yang^{1,2}, Chen Hu^{3,2}, Yan-Mei Chen^{1,2} and Jian-Min Wang¹

¹ Key Laboratory for Particle Astrophysics, Institute of High Energy Physics, Chinese Academy of Sciences, Beijing 100049; yangfang@mail.ihep.ac.cn

² Graduate School of Chinese Academy of Sciences, Beijing 100049

³ National Astronomical Observatories, Chinese Academy of Sciences, Beijing 100012

Received 2006 July 28; accepted 2006 October 11

Abstract We compiled a sample of 98 radio-quiet active galactic nuclei observed by *ASCA*, *Chandra*, *XMM-Newton*, *INTEGRAL* and *Swift* with the aim of testing the formation of hot corona and the magnetic shear stress operating in a disk-corona system. We found a strong correlation between the hard X-ray luminosity, bolometric luminosity L_{Bol} and Eddington luminosity L_{Edd} , in the sense that the fraction f of hard X-ray to the bolometric luminosity is inversely proportional to the Eddington ratio. This correlation favors the shear stress tensor being of the form of $t_{r\phi} \propto P_{\text{gas}}$, with which the disk-corona structure is stable.

Key words: accretion, accretion disks — galaxies: active — magnetic fields

1 INTRODUCTION

A phenomenological model of disk-corona was built up based on the hard X-ray emission from Cyg X-1 (Liang et al. 1977). It is usually assumed that, in active galactic nuclei, a fraction f of total dissipated energy is transferred vertically outside the disk, and released in the hot, magnetically dominated corona (Haardt & Maraschi 1991; Svensson & Zdziarski 1994, hereafter SZ94). However, the undergoing physics of the factor f is poorly understood.

Magnetic field turbulence produced by Magneto-rotational instability (MRI, Velikhov 1959; Balbus & Hawley 1991) is believed to play an important role in the transportation of angular momentum (Balbus & Hawley 1991; Tout & Pringle 1992; Brandenburg et al. 1995; Hawley et al. 1996; Balbus 2003; Turner et al. 2003). Shakura & Sunyaev (1973, hereafter SS73) first assumed that angular momentum transport was carried out by turbulence and that the stress tensor was scaled to the disk pressure, $t_{r\phi} = \alpha P$, α being the viscosity. Other scalings of the viscous stress $t_{r\phi}$ have been discussed (e.g. Taam & Lin 1984; Burm 1985; Merloni & Fabian 2002, hereafter MF02; Watarai & Mineshige 2003) after SS73. On the other hand, numerical simulations find that the viscous stress is generally proportional to the magnetic pressure (Hawley et al. 1995). Therefore, it is important to determine how the magnetic pressure depends on the gas pressure, radiation pressure or both. However, numerical studies have not given a clear answer to this question (e.g. Honma et al. 1991; Hawley et al. 1995; Sano et al. 2004) since the physical processes inside the disks are very complicated (Balbus & Hawley 1991; Machida & Matsumoto 2003; Kato et al. 2004). Many authors considered the following prescription for the viscous stress, $t_{r\phi} = \alpha P_{\text{tot}}^{1-\mu/2} P_{\text{gas}}^{\mu/2}$ (Szuszkiewicz 1990; Honma et al. 1991; Merloni & Nayakshin 2006), where μ can take any value between 0 and 2. These theoretical results should be tested by observational data.

It has been realized that the magnetic field turbulence may also play important roles in the formation of hot corona (Galeev et al. 1979; Stella & Rosner 1984, hereafter SR84; MF02; Kuncic & Bicknell 2004). SR84 argued that the strong buoyancy and magnetic field reconnection inevitably lead to the formation of

* Supported by the National Natural Science Foundation of China.

hot corona. If magnetic stress and energy transportation are assumed, then the factor f can be calculated (MF02). Thus the working viscous stress can be tested from hard X-ray observations. Wang et al. (2004, hereafter W04) compiled a sample of 56 radio-quiet AGNs from ASCA observations and found that the ratio $F_x \equiv L_{2-10 \text{ keV}}/L_{\text{bol}}$ strongly correlates with the Eddington ratio $\varepsilon = L_{\text{Bol}}/L_{\text{Edd}}$ as $F_x \propto \varepsilon^{-0.64 \pm 0.09}$, $L_{\text{Edd}} = 4\pi c GM_{\text{BH}}/\kappa_{\text{es}}$ ($\kappa_{\text{es}} = 0.34$) being the Eddington luminosity. The correlation favors the magnetic stress $t_{r\phi} \propto P_{\text{gas}}$. However, the sample is small and it only includes the 2 – 10 keV data. Hard X-ray emission extending to 150 keV are available detected by *INTEGRAL* and *Swift* (Markwardt et al. 2005; Bassani et al. 2006). Obviously, the new data will set more stringent constraints on disk-corona models.

In this paper, we extend the study of W04 by including more samples, new data and deliberated theoretical models to test the proper magnetic stress when coupled with formation of hot corona and radial advection. We find that the current data favor the shear stress tensor in the form of $t_{r\phi} = -\alpha P_{\text{gas}}$.

2 OBSERVATIONAL CONSTRAINTS

We assemble the data of Seyfert 1 galaxies and PG quasars from the literature. The sample covers broad line Seyfert 1 galaxies, narrow line Seyfert 1 galaxies and PG quasars. Since objects in the present sample tend to be pole-on sources, the anisotropic effects of radiation from the disks can be neglected. The present sample consists of 98 radio-quiet AGNs. Among them 89 sources have $L_{2-10 \text{ keV}}$ given by ASCA observations from the Tartarus database, Turner et al. (1999), Vaughan et al. (1999), Reeves & Turner (2000) and Leighly (1999), and nine sources have observations by *INTEGRAL* and *Swift*.

Table 1 gives the data of the present sample. Col. (1) gives the name of objects; Col. (2) the redshift; (3) the photon index between 2 and 10 keV; Col. (4) the 2–10 keV luminosity of the object unless otherwise specified; Col. (5) the luminosity between 2 and 150 keV in erg, extrapolated from Col. (4); Col. (6) the black hole mass; Col. (7) the bolometric luminosity in erg; Col. (8) the logarithm of the ratio of the 2–150 keV luminosity to the bolometric luminosity; Col. (9) the logarithm of the Eddington ratio; Col. (10) the references of the X-ray luminosity, the black hole mass and the bolometric luminosity. All the data have been reduced to the cosmology of Hubble constant $H_0 = 75 \text{ km s}^{-1}\text{Mpc}^{-1}$ and the deceleration factor $q_0 = 0.5$.

A key parameter in the examination of the disk-corona model is the black hole mass. There are several ways to estimate the black hole mass: 1) the reverberation mapping method (Kaspi et al. 2000; Peterson et al. 2004); 2) the empirical reverberation relation (Kaspi et al. 2000; Vestergaard 2002), which gives

$$R_{\text{BLR}} = 32.9 \left[\frac{\lambda L_{\lambda}(5100\text{\AA})}{10^{44} \text{erg s}^{-1}} \right]^{0.7} \text{lt} - d, \quad (1)$$

where R_{BLR} is the radius of the broad line region, then the black hole masses are given by

$$M_{\text{BH}} = 1.5 \times 10^5 \left(\frac{R_{\text{BLR}}}{\text{lt} - \text{days}} \right) \left(\frac{v_{\text{FWHM}}}{10^3 \text{km s}^{-1}} \right)^2 M_{\odot}. \quad (2)$$

The black hole masses in Table 1 are taken from Woo & Urry (2002, hereafter WU02), otherwise M_{BH} is estimated by the BLR Size-Luminosity Relation. $L_{5100\text{\AA}}^{\circ}$ is obtained from the apparent magnitude m_V given in Véron-Cetty & Véron (2003) quasar catalog (11th edition) through an extrapolation of a power law spectrum in optical band as $F_{\nu} \propto \nu^{-0.5}$ (Vestergaard 2002). The bolometric luminosity L_{Bol} is taken from WU02 and Grupe et al. (2004), otherwise it is estimated via $L_{\text{Bol}} = 9L_{5100\text{\AA}}^{\circ}$ (Kaspi et al. 2000).

Using two-variable correlation analysis, we find the correlation between $L_{2-10 \text{ keV}}$, L_{Edd} and L_{Bol} to be

$$\log L_{2-10 \text{ keV}} = (0.53 \pm 0.08) \log L_{\text{Bol}} + (0.23 \pm 0.08) \log L_{\text{Edd}} + (9.4 \pm 5.2), \quad (3)$$

with the Pearson's coefficient $r = 0.81$ and $F(2, 87) = 80.7$ in the F -test. The goodness of the fit is shown in the left panel of Figure 1. Converting this relation in terms of the Eddington ratio, we rewrite Equation (3) as

$$\log \frac{L_{2-10 \text{ keV}}}{L_{\text{Bol}}} = -0.47 \log \varepsilon - 0.24 \log L_{\text{Edd}} + 9.4. \quad (4)$$

This equation shows that the factor f decreases with the Eddington ratio, that is, the corona gets weaker as the Eddington ratio increases. It is very interesting that the hot corona is mainly controlled by the Eddington

ratio rather than by the black hole mass. Equation (4) shows a weak dependence on the black hole mass, as shown by the scatter in the relation between f and the Eddington ratio (the right panel of Fig. 1). This is similar to previous finding in W04.

There are nine sources that have observations of *INTEGRAL* (Bassani et al. 2006) and *Swift* (Markwardt et al. 2005), and we can obtain the black hole mass and bolometric luminosity. We extrapolate the luminosity of all the 98 sources into the 2–150 keV luminosity. The flux in $E_1 - E_2$ band $F_{E_1-E_2} = \int_{E_1}^{E_2} K (E/1 \text{ keV})^{-\Gamma} E dE$, where K is a coefficient, Γ is the photon index. As $L_{2-150 \text{ keV}}/L_{E_1-E_2} = F_{2-150 \text{ keV}}/F_{E_1-E_2} = \int_2^{150} E^{-\Gamma+1} dE / \int_{E_1}^{E_2} E^{-\Gamma+1} dE$, we can extrapolate luminosity of $E_1 - E_2$ band into that of 2 – 150 keV by

Table 1 The Sample

Object	z	Γ	$\log L_{X,\text{obs}}^{\text{a}}$	$\log L_{2-150 \text{ keV}}$	$\log M_{\text{BH}}$	$\log L_{\text{Bol}}$	$\log \left(\frac{L_{2-150 \text{ keV}}}{L_{\text{Bol}}} \right)$	$\log \left(\frac{L_{\text{Bol}}}{L_{\text{Edd}}} \right)$	Ref.
(1)	(2)	(3)	(erg)	(erg)	(M_{\odot})	(7)	(8)	(9)	(10)
1H 0707–495	0.041	2.27	42.50	42.80	6.46	44.63	-1.83	0.07	1
2RE J2248–512	0.100	–	43.93	44.42	7.94	45.70	-1.27	-0.35	3
Akn 120	0.032	1.91	44.07	44.55	8.27	44.91	-0.36	-1.46	1,7
Akn 564	0.025	2.70	43.39	43.54	6.30	44.81	-1.27	0.41	1
B2 1425+26	0.366	–	44.91	45.40	9.36	46.60	-1.20	-0.86	6
ESO 198–G24	0.046	1.78	43.66	44.23	8.48	45.22	-0.99	-1.36	12
ESO 209–G012	0.040	–	43.92 ^b	44.28	7.99	44.77	-0.49	-1.32	5,18
ESO 323–G077	0.015	–	43.11 ^b	43.47	7.34	44.75	-1.28	-0.69	5,19
ESO 511–G030	0.022	–	43.68 ^b	44.04	7.68	44.41	-0.36	-1.37	5,20
EXO 055625–3838.6	0.034	1.70	43.97	44.60	7.21	44.37	0.23	-0.94	1
EXO 055620–3820.2	0.034	–	44.2 ^c	44.34	7.34	44.75	-0.42	-0.68	10,19
EXO 1128.1+6908	0.043	–	43.19	43.68	7.26	44.84	-1.16	-0.52	3
F 9	0.046	1.91	43.97	44.46	7.91	45.23	-0.77	-0.78	7
F 1146	0.031	–	43.54 ^b	43.90	7.28	44.00 ^d	-0.10	-1.38	5,21,22
HE 1029–1401	0.086	1.81	44.39	44.94	9.11	46.02	-1.08	-1.19	6
IC 4329A	0.016	1.71	43.06	43.68	6.77	44.78	-1.10	-0.09	7,1
IRAS 13224–3809	0.067	1.97	42.60	43.04	6.86	45.80	-2.75	0.84	1
IRAS 13349+2438	0.107	2.31	44.07	44.35	8.14	45.76	-1.41	-0.48	3
IRAS 17020+4544	0.060	2.20	43.74	44.06	6.54	44.74	-0.68	0.10	8
IRAS 20181–2244	0.185	2.33	43.87	44.14	6.80	45.43	-1.29	0.53	8,11
Kaz 163	0.063	1.92	43.19	43.67	7.11	45.02	-1.35	-0.19	13
LB 1727	0.104	1.56	44.24	44.98	8.02	45.69	-0.71	-0.43	3
MCG+04-22-042	0.032	–	43.9 ^c	44.04	7.42	44.77	-0.73	-0.75	10,14
MCG+08-11-011	0.020	1.56	43.19	43.93	7.44	44.43	-0.50	-1.10	1
MCG-01-13-025	0.016	–	43.3 ^c	43.44	7.92	44.42	-0.97	-1.60	10,18
MCG-06-30-015	0.008	2.02	42.72	43.14	6.50	44.04	-0.90	-0.56	1
MR 2251–178	0.064	1.67	44.40	45.05	8.01	45.40	-0.35	-0.71	12
Mrk 6	0.019	–	43.48 ^b	43.84	8.02	44.56	-0.72	-1.56	5,17
Mrk 42	0.025	2.14	42.54	42.89	5.61	43.91	-1.02	0.20	1
Mrk 110	0.036	–	43.84	44.33	6.82	44.71	-0.38	-0.21	7
Mrk 142	0.045	2.12	43.18	43.54	6.65	44.55	-1.01	-0.20	13
Mrk 205	0.071	1.80	43.89	44.45	8.32	45.82	-1.37	-0.60	12
Mrk 279	0.030	2.04	43.99	44.40	7.83	44.55	-0.15	-1.38	1
Mrk 290	0.030	1.68	43.18	43.82	7.27	44.65	-0.83	-0.72	1
Mrk 335	0.026	1.94	43.42	43.88	6.69	44.69	-0.81	-0.10	7,1
Mrk 359	0.017	1.88	42.43	42.93	6.55	43.55	-0.62	-1.10	12
Mrk 507	0.056	1.61	42.62	43.32	6.34	44.54	-1.22	0.10	8
Mrk 509	0.035	1.82	44.03	44.57	7.86	45.03	-0.46	-0.93	7
Mrk 705	0.028	–	43.19	43.68	7.13	44.74	-1.05	-0.49	2
Mrk 766	0.013	2.16	43.08	43.42	6.05	44.23	-0.81	0.08	3,1
Mrk 896	0.026	2.04	42.64	43.04	6.79	43.89	-0.85	-1.00	12
Mrk 926	0.047	1.73	44.15	44.76	8.69	45.53	-0.77	-1.26	1
Mrk 1040	0.017	1.56	42.83	43.57	7.64	44.53	-0.96	-1.21	7,1
Mrk 1044	0.016	2.48	42.49	42.70	7.28	44.20	-1.50	-1.18	12
Mrk 1383	0.086	–	44.04	44.53	8.75	45.78	-1.25	-1.07	12
Nab 0205+024	0.155	2.27	44.52	44.81	7.86	45.45	-0.64	-0.51	7,1

Table 1 (Continued)

Object	z	Γ	$\log L_{X,\text{obs}}^{\text{a}}$	$\log L_{2-150\text{keV}}$	$\log M_{\text{BH}}$	$\log L_{\text{Bol}}$	$\log \left(\frac{L_{2-150\text{keV}}}{L_{\text{Bol}}} \right)$	$\log \left(\frac{L_{\text{Bol}}}{L_{\text{Edd}}} \right)$	Ref.
(1)	(2)	(3)	(4)	(5)	(6)	(7)	(8)	(9)	(10)
NGC 3227	0.004	1.61	42.01	42.71	6.76	43.86	-1.15	-1.00	1
NGC 3516	0.009	1.83	43.43	43.97	7.36	44.29	-0.32	-1.17	7,1
NGC 3783	0.009	1.70	42.88	43.51	6.94	44.41	-0.90	0.63	7
NGC 4051	0.002	1.93	41.12	41.59	6.13	43.56	-1.97	-0.67	7
NGC 4151	0.003	1.57	43.01	43.74	7.13	43.73	0.01	-1.50	7,1
NGC 4593	0.009	1.78	42.69	43.26	6.91	44.09	-0.83	-0.92	7
NGC 5548	0.017	1.79	43.76	44.32	8.03	44.83	-0.51	-1.30	7,1
NGC 6814	0.005	—	42.52 ^b	42.89	7.28	43.92	-1.03	-1.46	5,7
NGC 7213	0.006	—	42.29	42.78	7.99	44.30	-1.52	-1.79	7
NGC 7469	0.017	1.91	43.22	43.71	6.84	45.28	-1.57	0.34	7
PDS 456	0.184	—	44.71	45.20	8.91	46.90	-1.70	-0.11	12
PG 0050+124	0.061	2.28	43.83	44.12	7.26	45.47	-1.35	0.11	4
PG 0157+001	0.163	2.10	43.79	44.16	8.03	45.62	-1.46	-0.51	4,7
PG 0804+761	0.100	2.05	44.40	44.60	8.84	45.75	-1.15	-1.01	15,7
PG 0844+349	0.064	2.11	43.68	43.66	7.97	45.36	-1.70	-0.71	15,7
PG 0947+396	0.206	1.81	44.29	44.84	8.58	45.77	-0.93	-0.97	16
PG 0953+414	0.234	2.01	44.67	44.94	8.44	46.16	-1.22	-0.20	15,3
PG 1001+054	0.161	—	43.05	43.54	7.70	45.76	-2.22	-0.08	16
PG 1048+342	0.167	1.77	43.98	44.73	8.28	45.51	-0.78	-0.73	16
PG 1114+445	0.144	1.48	44.10	44.82	8.41	45.60	-0.78	-0.97	4
PG 1115+407	0.154	2.16	43.87	44.21	7.51	45.80	-1.59	0.19	3
PG 1116+215	0.177	2.14	44.43	44.79	8.50	46.58	-1.79	0.00	4,3
PG 1202+281	0.165	1.69	44.37	45.01	8.12	45.39	-0.38	-0.83	4,7
PG 1211+143	0.081	1.76	43.64	44.29	8.16	45.83	-1.55	-0.33	15,3
PG 1216+069	0.331	1.73	44.62	44.68	9.17	46.52	-1.85	-0.82	4
PG 1244+026	0.048	2.55	43.09	42.29	6.29	44.62	-2.33	0.35	4,3
PG 1307+085	0.155	1.46	44.02	44.85	8.64	46.05	-1.20	-0.69	15,3
PG 1322+659	0.168	2.20	43.97	44.29	8.15	45.77	-1.48	-0.48	3
PG 1352+183	0.152	1.91	44.07	44.55	8.27	45.63	-1.08	-0.74	4
PG 1402+261	0.164	2.06	44.09	44.48	7.59	46.13	-1.65	0.44	3
PG 1404+226	0.098	2.30	44.40	43.20	6.79	45.35	-2.15	0.37	2
PG 1411+442	0.090	0.38	43.34	45.28	8.65	45.58	-0.30	-1.17	15,7
PG 1415+451	0.114	2.03	43.54	43.95	7.81	45.37	-1.42	-0.54	4
PG 1416-129	0.129	1.78	44.48	45.05	8.50	45.90	-0.85	-0.70	4,9
PG 1427+480	0.221	1.90	44.14	44.63	8.02	45.78	-1.15	-0.40	16
PG 1440+356	0.079	2.03	43.70	44.11	7.30	45.37	-1.26	-0.03	4
PG 1444+407	0.267	2.12	44.05	44.46	8.23	46.28	-1.82	-0.40	4,7
PG 1501+106	0.036	1.88	43.63	44.13	7.88	45.12	-0.99	-0.86	4
PG 1543+489	0.400	2.46	44.16	44.38	7.79	46.11	-1.73	0.22	8
PG 1613+658	0.129	1.70	44.19	44.82	8.45	45.66	-0.84	-0.89	15,7
PG 1626+554	0.133	1.95	44.10	44.56	8.13	45.85	-1.29	-0.38	3
PG 1700+518	0.290	—	43.90	44.39	8.31	46.56	-2.17	0.15	7
PG 2214+139	0.066	0.94	43.62	44.95	8.35	45.45	-0.50	-1.00	2
PHL 909	0.171	1.11	44.24	45.40	8.90	45.47	-0.07	-1.53	7
PHL 1092	0.396	1.99	44.10	44.53	7.61	46.07	-1.54	0.36	8
PKS 0558-504	0.137	1.81	44.67	45.22	7.56	45.80	-0.58	0.14	8
Q 0056-363	0.162	2.03	44.17	44.58	8.95	46.30	-1.72	-0.75	12
RX J01484-2758	0.120	2.06	43.39	43.78	7.19	45.64	-1.86	0.35	3
RX J0439.7-4540	0.224	2.25	44.04	44.34	7.12	45.66	-1.32	0.44	8
RE J1034+393	0.042	2.35	43.05	43.31	6.45	44.52	-1.21	-0.03	3,1
TON S180	0.062	2.46	43.58	43.79	7.04	45.51	-1.72	0.37	3
Was 61	0.045	—	43.26	43.75	7.03	44.83	-1.08	-0.30	3

NOTE ^a Luminosity in the 2–10 keV band if there is no special note.^b INTEGRAL luminosity in the 20–100 keV band (Bassani et al. 2006).^c SWIFT/BAT luminosity in the 14–195 keV band (Markwardt et al. 2005).^d Bolometric luminosity estimated via $L_{\text{5100}\text{\AA}}$, where $L_{\text{5100}\text{\AA}}$ is obtained from M_{B} .

REFERENCES (1) Turner et al. (1999); (2) Boroson & Green (1992); (3) Grupe et al. (2004); (4) Vestergaard (2002); (5) Bassani et al. (2006); (6) Wandel (2002); (7) Woo & Urry (2002); (8) Vaughan et al. (1999); (9) Reeves & Turner (2000); (10) Markwardt et al. (2005); (11) Elizalde & Steiner (1994); (12) Page et al. (2004); (13) Leighly (1999); (14) Bade et al. (1995); (15) Peterson (2004); (16) Shields (2003); (17) Sergeev et al. (1999); (18) Pietsch et al. (1998); (19) Winkler et al. (1992); (20) Fischer et al. (1998); (21) Zimmermann et al. (2001); (22) Crenshaw et al. (2003).

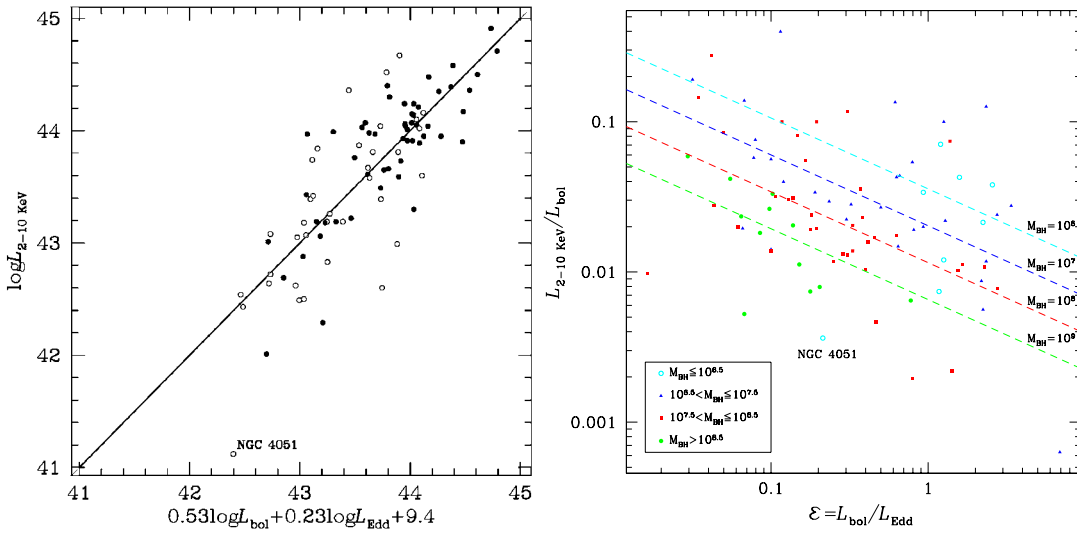


Fig. 1 Left: Correlation between $L_{2-10 \text{ keV}}$ and a combination of L_{Bol} and L_{Edd} in our sample. The open and filled circles represent the NLS1s (FWHM H β < 2000 km s $^{-1}$) and the BLS1s, respectively. Right: Transformed correlation between the flux ratio and the Eddington ratio.

$$\log L_{2-150 \text{ keV}} = \log L_{E_1-E_2} + \log \int_{E_1}^{150} E^{-\Gamma+1} dE - \log \int_{E_1}^{E_2} E^{-\Gamma+1} dE, \quad (5)$$

where $E_1 = 2$, $E_2 = 10$ for *ASCA* data, $E_1 = 20$, $E_2 = 100$ for *INTEGRAL* data and $E_1 = 14$, $E_2 = 195$ for *Swift* data. In the extrapolation, we use the photon index of the source if it has been given. Otherwise, the photon index is fixed at 1.9. We find the correlation between $L_{2-150 \text{ keV}}$, L_{Edd} and L_{Bol} to be

$$\log L_{2-150 \text{ keV}} = (0.34 \pm 0.081) \log L_{\text{Bol}} + (0.49 \pm 0.077) \log L_{\text{Edd}} + (6.5 \pm 5.1), \quad (6)$$

with the Pearson's coefficient $r = 0.82$ and $F(2, 95) = 94.0$ of the F -test. It is consistent with the relation between $L_{2-10 \text{ keV}}$, L_{Edd} and L_{Bol} . The goodness of the fit is shown in the left panel of Figure 2. Converting this relation in terms of the Eddington ratio, we rewrite Equation (6) as

$$\log \frac{L_{2-150 \text{ keV}}}{L_{\text{Bol}}} = -0.66 \log \epsilon - 0.17 \log L_{\text{Edd}} + 6.5. \quad (7)$$

The right panel of Figure 2 shows the result of Equation (7).

In our sample, 78 sources have observed photon indices in 2 – 10 keV band. We test the correlation between Γ and the Eddington ratio for our sample (excluding two sources (PG 2214+139 and PG 1411+442) with photon indexes smaller than 1). We find

$$\Gamma = (0.31 \pm 0.043) \log \epsilon + (2.1 \pm 0.032),$$

with correlation coefficient $r = 0.64$ and $F(1, 74) = 51.0$ of the F -test (Fig. 3). This is consistent with previous finding in W04. This relation could be used as an indicator of Eddington ratio for high redshift quasars with measured photon index Γ (Shemmer et al. 2006).

3 THEORETICAL MODELS OF DISK-CORONA

In this part, we solve the structure of the disk in the disk-corona system including radial advection, and focus on testing the working of magnetic viscous stress via the correlation between the factor f and the Eddington ratio obtained from our sample.

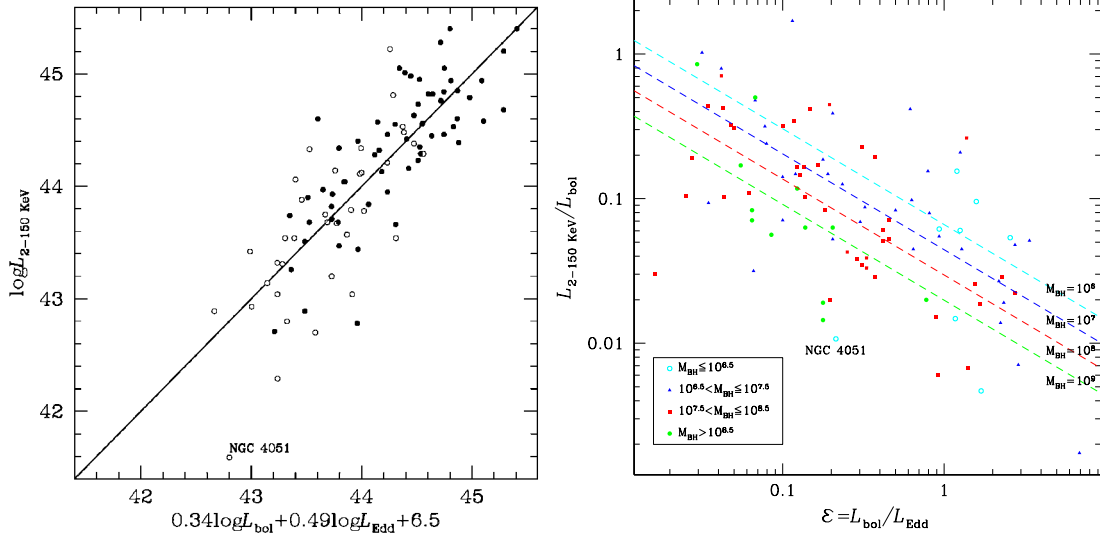


Fig. 2 Left: Correlation between $L_{2-150 \text{ keV}}$ and a combination of L_{bol} and L_{Edd} in our sample. The open and filled circles represent the NLS1s ($\text{FWHM H}\beta < 2000 \text{ km s}^{-1}$) and the BLS1s, respectively. Right: Transformed correlation between the flux ratio and the Eddington ratio.

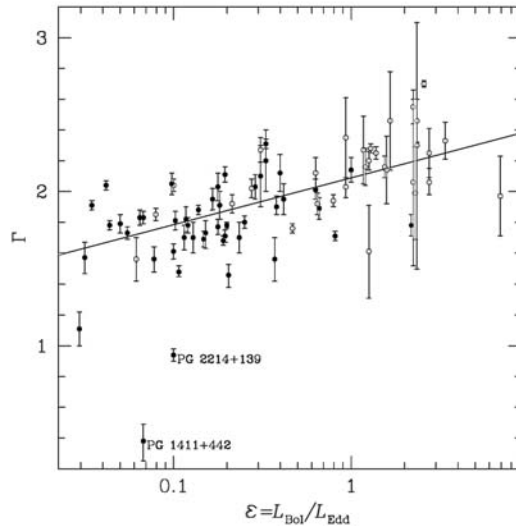


Fig. 3 The 2 – 10 keV X-ray photon spectral index Γ vs. the Eddington ratio ε relation. The open and filled circles represent the NLS1s ($\text{FWHM H}\beta < 2000 \text{ km s}^{-1}$) and the BLS1s, respectively.

3.1 Basic Equations of Disk-Corona

We follow the model of SZ94, but allowing the factor f to be a function of radius from the black hole and taking advection cooling into consideration. Assuming the cold disk is geometrically thin and the hydrostatic equilibrium holds in the vertical direction, we have

$$H = \frac{c_s}{\Omega_K}, \quad (8)$$

where $c_s^2 = P_{\text{tot}}/\rho$. Angular momentum conservation in the ϕ -direction is

$$-t_{r\phi} = \frac{\Omega_K}{4\pi H} \dot{M} \mathcal{J}(R), \quad (9)$$

where $t_{r\phi}$ is the torques acting on the cold disk, which transports the angular momentum outward. The inner bounding function is $\mathcal{J}(R) \equiv (1 - \sqrt{3R_s/R})$, where $R_s = 2GM/c^2$ is the Schwarzschild radius of a black hole of mass M . The energy equation reads

$$Q_{\text{rad}} + Q_{\text{adv}} = (1 - f)Q, \quad (10)$$

where Q_{rad} , Q_{adv} and Q are the radiative cooling, advection cooling, viscous heat energy flux density, respectively,

$$Q_{\text{rad}} = \frac{2c}{\xi} \frac{P_{\text{rad}}}{\tau}, \quad (11)$$

$$Q_{\text{adv}} = \frac{\dot{M}}{2\pi R^2} \frac{P_{\text{tot}}}{\rho} \xi_a, \quad (12)$$

$$Q = \frac{3\Omega_K^2}{8\pi} \dot{M} \mathcal{J}(R), \quad (13)$$

$$P_{\text{tot}} = P_{\text{gas}} + P_{\text{rad}} = 2\rho \frac{k}{m_p} T + \frac{aT^4}{3}, \quad (14)$$

where P_{tot} , ρ , T , H and τ are the total pressure, mass density, temperature, pressure scale height and scattering optical depth of the cold disk, respectively, $\Omega_K = (GM/R^3)^{1/2}$ is the Keplerian angular velocity, and ξ_a is the advection cooling parameter. In this paper, the magnetic pressure is not included in P_{tot} , following Merloni (2003).

If we know f and $t_{r\phi}$, we can solve Equations (8)–(14) and obtain severally the total pressure, mass density, temperature, pressure scale height and scattering optical depth of the cold disk.

3.2 Magnetic Viscous Stress and Corona

Assuming that the energy transportation from the cold disk to the hot corona is a result of the buoyancy that drives the magnetic tubes across the extent of the disk, the fraction of the energy so transported is $f = P_{\text{mag}} v_P / Q$, where v_P is the transporting velocity, $P_{\text{mag}} = B^2/8\pi$ is the magnetic pressure. The dissipated energy flux density is $Q = -(3/2)c_s t_{r\phi}$ (MF02). Since numerical studies have shown that the viscous stress scales with magnetic pressure, we assume $t_{r\phi} = -k_0 P_{\text{mag}}$. So we have

$$f = \frac{2v_P}{3k_0 c_S} = \frac{2^{3/2} b}{3k_0} \sqrt{\frac{P_{\text{mag}}}{P_{\text{tot}}}} = \frac{2^{3/2} b}{3k_0^{3/2}} \sqrt{\frac{(-t_{r\phi})}{P_{\text{tot}}}} \equiv C \sqrt{\frac{(-t_{r\phi})}{P_{\text{tot}}}}, \quad (15)$$

where $b = v_P/v_A$, $v_A = B/\sqrt{4\pi\rho}$ is the Alfvén velocity, $P_{\text{tot}} = P_{\text{rad}} + P_{\text{gas}}$, $c_s^2 = P_{\text{tot}}/\rho$ and $C \equiv 2^{3/2} b / (3k_0^{3/2})$. The parameter b is related to the efficiency of the buoyant transport, and is of the order of unity for extremely evacuated tubes. Similar to Merloni (2003), we take $C = 1$ in the following.

When building the disk-corona system, an expression for the shear stress $t_{r\phi}$ is needed. Hydromagnetic turbulent viscosity is considered as the cause of the shear stress. However, there is no a consistent theory of turbulence. Different expressions for the shear stress have been considered. Here, we check six distinct types of magnetic stresses.

1) SS73 introduced a phenomenological prescription of the shear stress $t_{r\phi} = -\alpha P_{\text{tot}}$ to establish contact with the observations, because the physical process of the viscous stress is poorly understood. Using Equation (15),

$$f = C\alpha^{\frac{1}{2}}. \quad (16)$$

The inner, radiation pressure dominated region of an accretion disk with this scaling is thermally and viscously unstable (Pringle et al. 1973; Lightman & Eardley 1974; Pringle 1976; Shakura & Sunyaev 1976).

Equation (16) shows that the factor f is independent of the accretion rate and black hole mass. Equation (7) could rule out this viscous law.

2) It has been argued that the growth of the magnetic field may be controlled by buoyancy and the magnetic stress is then scaled to the gas pressure, i.e. $t_{r\phi} = -\alpha P_{\text{gas}}$ (Lightman & Eardley 1974; Coroniti 1981; Meyer & Meyer-Hofmeister 1982; SR84; Burm 1985). In this case,

$$f = C\alpha^{\frac{1}{2}} \left(\frac{P_{\text{gas}}}{P_{\text{tot}}} \right)^{\frac{1}{2}}. \quad (17)$$

3) We consider the case that $t_{r\phi}$ is scaled to the radiation pressure, $t_{r\phi} = -\alpha P_{\text{rad}}$, then we have

$$f = C\alpha^{\frac{1}{2}} \left(\frac{P_{\text{rad}}}{P_{\text{tot}}} \right)^{\frac{1}{2}}. \quad (18)$$

4) We also consider the case that $t_{r\phi} = -\alpha\sqrt{P_{\text{rad}}P_{\text{tot}}}$. When $P_{\text{rad}} \gg P_{\text{gas}}$ (low accretion rates), $t_{r\phi} \approx -\alpha P_{\text{rad}}$ (model 3). When $P_{\text{rad}} \ll P_{\text{gas}}$ (high accretion rates), $t_{r\phi} \approx -\alpha\sqrt{P_{\text{rad}}P_{\text{gas}}}$ (model 6). We obtain

$$f = C\alpha^{\frac{1}{2}} \left(\frac{P_{\text{rad}}}{P_{\text{tot}}} \right)^{\frac{1}{4}}. \quad (19)$$

5) Ichimaru (1975) pointed out that the growth of the magnetic field may be controlled by reconnection and suggest $t_{r\phi} = -\alpha\sqrt{P_{\text{gas}}P_{\text{tot}}}$. This form of stress has been studied by many authors (Taam & Lin 1984; Burm 1985; Lin & Shields 1986; Szuszkiewicz 1990; MF02). Based on an analytical work (Blaes & Socrates 2001) and a three-dimensional MHD numerical simulation (Turner et al. 2003) of magneto-rotational instability in radiative accretion disks, this formulation can be derived (MF02; Merloni 2003). Then we obtain

$$f = C\alpha^{\frac{1}{2}} \left(\frac{P_{\text{gas}}}{P_{\text{tot}}} \right)^{\frac{1}{4}}. \quad (20)$$

6) Laor & Netzer (1989) investigated the structure and the spectrum of an α -disk assuming $t_{r\phi} = -\alpha\sqrt{P_{\text{rad}}P_{\text{gas}}}$,

$$f = C\alpha^{\frac{1}{2}} \left(\frac{P_{\text{gas}}P_{\text{rad}}}{P_{\text{tot}}^2} \right)^{\frac{1}{4}}. \quad (21)$$

Specifying the magnetic stress and assuming $\xi_a = 5$, Equations (8)–(15) can be solved numerically to calculate f at every radius r for every accretion rate \dot{m} when M_{BH} and α are specified. Figure 4 shows the $f - r$ relation for $\dot{m} = 0.1$ when $M_{\text{BH}} = 10^8$ and $\alpha = 0.1$.

One can see from Figure 4 that, from the out disk region to the inner disk region, f in models 2 and 5 first decreases and then increases while an opposite variation shows up in models 3, 4 and 6. Factor f is determined by the ratio $P_{\text{gas}}/P_{\text{tot}}$ (models 2, 5 and 6) or the ratio $P_{\text{rad}}/P_{\text{tot}}$ (models 3, 4 and 6). In the out region of the disk, where P_{gas} is dominant, $P_{\text{gas}}/P_{\text{tot}} \simeq 1$ and $P_{\text{rad}}/P_{\text{tot}}$ is small. Then from the out to inner disk region, the ratio $P_{\text{gas}}/P_{\text{tot}}$ decreases and $P_{\text{rad}}/P_{\text{tot}}$ increases until radial advection becomes dominant.

Current data only allow us to test the fraction f as a global parameter of the disk-corona system. We thus define an averaged value $\langle f \rangle$ as in MF02:

$$\langle f \rangle = \frac{\int_3^\infty f(r)Q(r)2\pi r dr}{\int_3^\infty Q(r)2\pi r dr}. \quad (22)$$

As W04 pointed out, the $\langle f \rangle - \dot{m}$ relation is not sensitive to the value of M_{BH} and α (the right panel of Fig. 5 shows only models 2 and 5 for clarity). The slope of the $\langle f \rangle - \dot{m}$ relation is only sensitive to the form of the shear stress, so we are able to test the shear stress model by the $\langle f \rangle - \dot{m}$ relation.

The left panel of Figure 5 shows $\langle f \rangle$ as a function of the accretion rate for different shear stress models. The value of the fraction f in model 1 relates to a constant α and is the same at all radii of the disk. In models

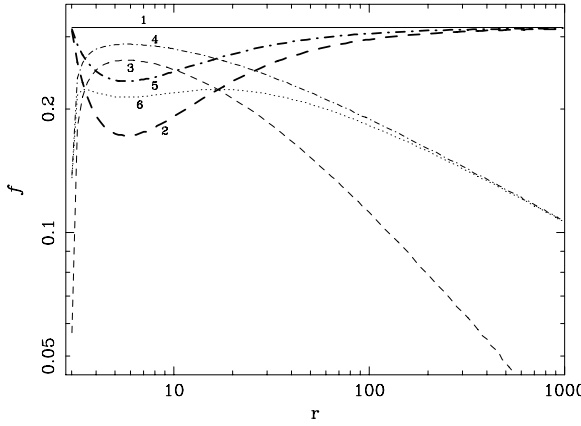


Fig. 4 f - r relations for six magnetic viscous stress models for $\dot{m} = 0.1$, $\alpha = 0.1$, $m_{\text{BH}} = 10^8$ and $\xi_a = 5$.

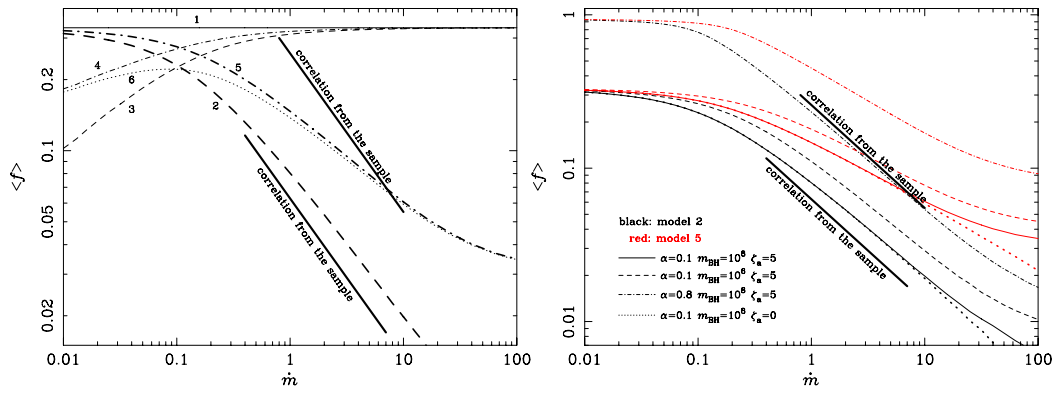


Fig. 5 Left: $\langle f \rangle - \dot{m}$ relation for the six magnetic viscous stress models with $\alpha = 0.1$, $m_{\text{BH}} = 10^8$ and $\xi_a = 5$, compared with our statistical result (thick solid). Right: $\langle f \rangle - \dot{m}$ relations of models 2 (black) and 5 (red) for $\alpha = 0.1$, $m_{\text{BH}} = 10^8$, $\xi_a = 5$ (solid), $\alpha = 0.1$, $m_{\text{BH}} = 10^6$, $\xi_a = 5$ (dashed), $\alpha = 0.8$, $m_{\text{BH}} = 10^8$, $\xi_a = 5$ (dotted) and $\alpha = 0.1$, $m_{\text{BH}} = 10^8$, $\xi_a = 0$ (dot-dashed).

Table 2 Different Models of Disk-corona System

Models	Advection	Viscous Stress	MC ^a	TI ^b	Consistent
C95	Yes	-	No	Yes	No
Janiuk02	Yes	$t_{r\phi} \propto P_{\text{tot}}$	Yes	Yes	Yes
MF02	No	$t_{r\phi} \propto \sqrt{P_{\text{gas}} P_{\text{tot}}}$	Yes	No	Yes
Janiuk04	Yes	$t_{r\phi} \propto P_{\text{gas}}$	Yes	Yes	Yes
W04	No	$t_{r\phi} \propto P_{\text{gas}}$	Yes	No	Yes
present	Yes	$t_{r\phi} \propto P_{\text{gas}}$	Yes	Yes	Yes

NOTE: ^a Yes or No according as magnetic reconnection is or is not considered

^b Yes or No according as the thermal instability of the disk is or is not discussed

3 and 4, $\langle f \rangle$ increases with \dot{m} . They are inconsistent with our statistical result. The $\langle f \rangle - \dot{m}$ relations in models 2, 5 and 6 are close to our statistical result, and obviously model 2 fits the best. This is consistent with the result of W04. A brief summary is given in Table 2.

As pointed out by previous investigators (e.g. Lightman & Eardley 1974), the inner disk region is thermally stable when $t_{r\phi} = -\alpha P_{\text{gas}}$. Including advection will make the inner region more stable.

4 CONCLUSIONS

We compiled a sample of 98 radio-quiet active galactic nuclei to test the magnetic shear stress that is operating in a disk corona system using the hard X-ray luminosity. We found a strong correlation between the hard X-ray luminosity, L_{Bol} and L_{Edd} , indicating that the fraction f of hard X-ray to the bolometric luminosity is inversely proportional to the Eddington ratio. This correlation favors the shear stress tensor being of the form of $t_{r\phi} \propto P_{\text{gas}}$. A more incisive test on the viscous stress requires larger samples of hard X-ray luminosity data. The global structure of accretion disk containing magnetic turbulence is worth investigating, and we will address it in a future work. For greater self-consistency, the disk-corona model should include the evolution of the magnetic field in the disk.

Acknowledgements This research has made use of the Tartarus (Version 3.1) database, created by Paul O'Neill and Kirpal Nandra at Imperial College London, and Jane Turner at NASA/GSFC. This research is supported by the NSFC through Grants 10325313, 10233030 and 10521001.

References

- Bade N., Fink H. H., Engels D. et al., 1995, *A&AS*, 110, 469
- Balbus S. A., Hawley J. F., 1991, *ApJ*, 376, 214
- Balbus S. A., 2003, *ARA&A*, 41, 555
- Bassani L., Molina M., Stephen J. B. et al., 2006, *ApJ*, 636, L65
- Blaes O., Socrates A., 2001, *ApJ*, 553, 987
- Boroson T. A., Green R. F., 1992, *ApJS*, 80, 109
- Brandenburg A., Nordlund A., Stein R. F. et al., 1995, *ApJ*, 446, 741
- Burm H., 1985, *A&A*, 143, 389
- Chen X., 1995, *ApJ*, 448, 803 (C95)
- Crenshaw D. M., Kraemer S. B., Gabel J. R., 2003, *AJ*, 126, 1690
- Coroniti F. V., 1981, *ApJ*, 244, 587
- Elizalde F., Steiner J. E., 1994, *MNRAS*, 268, L47
- Fischer J. -U., Hasinger G., Schuope A. D. et al., 1998, *Astron. Nachr.*, 319, 347
- Galeev A. A., Rosner R., Vaiana G. S., 1979, *ApJ*, 229, 318
- Grupe D., Wills B. J., Leighly K. M. et al., 2004, *AJ*, 127, 156
- Haardt F., Maraschi L., 1991, *ApJ*, 380, L51
- Hawley J. F., Gammie C. F., Balbus S. A., 1995, *ApJ*, 440, 742
- Hawley J. F., Gammie C. F., Balbus S. A., 1996, *ApJ*, 464, 690
- Honma F., Matsumoto R., Kato S., 1991, *PASJ*, 43, 147
- Ichimaru S., 1975, *ApJ*, 202, 528
- Janiuk A., Czerny B., Siemiginowska A., 2002, *ApJ*, 576, 908 (Janiuk02)
- Janiuk A., Czerny B., Siemiginowska A. et al., 2004, *ApJ*, 602, 595 (Janiuk04)
- Kato Y., Mineshige S., Shibata K., 2004, *ApJ*, 605, 307
- Kaspi S., Smith P. S., Netzer H. et al., 2000, *ApJ*, 533, 631
- Kuncic Z., Bicknell G. V., 2004, *ApJ*, 616, 669
- Laor A., Netzer H., 1989, *MNRAS*, 238, 897
- Leighly K. M., 1999, *ApJS*, 125, 317
- Liang E. P. T., Price R. H., 1977, *ApJ*, 218, 247
- Lightman A. P., Eardley D. M., 1974, *ApJ*, 187, L1
- Lin D. N. C., Shields G. A., 1986, *ApJ*, 305, 28
- Machida M., Matsumoto R., 2003, *ApJ*, 585, 429
- Markwardt C. B., Tueller J., Skinner G. K. et al., 2005, *ApJ*, 633, L77
- Merloni A., 2003, *MNRAS*, 341, 1051
- Merloni A., Fabian A. C., 2002, *MNRAS*, 332, 165 (MF02)
- Merloni A., Nayakshin S., 2006, *MNRAS*, 372, 278
- Meyer F., Meyer-Hofmeister E., 1982, *A&A*, 106, 34

- Page K. L., O'Brien P. T., Reeves J. N. et al., 2004, MNRAS, 347, 316
Peterson B. M., Ferrarese L., Gilbert K. M. et al., 2004, ApJ, 613, 682
Pietsch W., Bischoff K., Boller Th. et al., 1998, A&A, 333, 48
Pringle J. E., 1976, MNRAS, 177, 65
Pringle J. E., Rees M. J., Pacholczyk A. G., 1973, A&A, 29, 179
Reeves J. N., Turner M. J. L., 2000, MNRAS, 316, 234
Sano T., Inutsuka S., Turner N. J. et al., 2004, ApJ, 605, 321
Sergeev S. G., Pronik V. I., Sergeeva E. A. et al., 1999, AJ, 118, 2658S
Shakura N. I., Sunyaev R. A., 1973, A&A, 24, 337 (SS73)
Shakura N. I., Sunyaev R. A., 1976, MNRAS, 175, 613
Shemmer O., Brandt W. N., Netzer H. et al., 2006, ApJ, 646, L29
Shields G. A., Gebhardt K., Salviander S. et al., 2003, ApJ, 583, 124
Stella L., Rosner R., 1984, ApJ, 277, 312 (SR84)
Svensson R., Zdziarski A. A., 1994, ApJ, 436, 599 (SZ94)
Szuszkiewicz E., 1990, MNRAS, 244, 377
Taam R., Lin D. N. C., 1984, ApJ, 287, 761
Tout C. A., Pringle J. E., 1992, MNRAS, 259, 604
Turner T. J., George I. M., Nandra K. et al., 1999, ApJ, 524, 667
Turner N. J., Stone J. M., Krolik J. H. et al., 2003, ApJ, 593, 992
Vaughan S., Reeves J., Warwick R. et al., 1999, MNRAS, 309, 113
Velikhov E. P., 1959, Sov. Phys. JETP, 9, 995
Véron-Cetty M. -P., Véron P., 2003, A&A, 412, 399
Vestergaard M., 2002, ApJ, 571, 733
Wandel A., 2002, ApJ, 565, 762
Wang J. -M., Watarai K. -Y., Mineshige S., 2004, ApJ, 607, L107 (W04)
Watarai K. -Y., Mineshige S., 2003, ApJ, 596, 421
Winkler H., 1992, MNRAS, 257, 677
Woo J. -H., Urry C. M., 2002, ApJ, 579, 530 (WU02)
Zimmermann H. -U., Boller Th., Döbereiner S. et al., 2001, A&A, 378, 30